

## Article

# High-Sensitivity H<sub>2</sub> and CH<sub>4</sub> SAW Sensors with Carbon Nanowalls and Improvement in Their Performance after Plasma Treatment

Sorin Vizireanu <sup>1</sup>, Izabela Constantinoiu <sup>1,2</sup>, Veronica Satulu <sup>1</sup>, Silviu Daniel Stoica <sup>1</sup>  
and Cristian Viespe <sup>1,\*</sup>

<sup>1</sup> Laser Department, National Institute for Laser, Plasma and Radiation Physics, Atomistilor 409, RO-077125 Magurele, Romania; s\_vizi@infim.ro (S.V.); izabela.constantinoiu@inflpr.ro (I.C.); veronica.satulu@inflpr.ro (V.S.); daniel.stoica@inflpr.ro (S.D.S.)

<sup>2</sup> Faculty of Chemical Engineering and Biotechnologies, National University of Science and Technology Politehnica Bucharest, RO-011061 Bucharest, Romania

\* Correspondence: cristian.viespe@inflpr.ro

**Abstract:** We have developed surface acoustic wave (SAW) sensors with high sensitivity and a reversible response at room temperature (RT). The sensitive area of the sensor was prepared from vertically aligned graphene sheets, like carbon nanowalls (CNWs), which were deposited onto the quartz SAW sensor substrate. The CNWs were obtained by RF plasma-enhanced chemical vapor deposition (PECVD) at 600 °C, and their sensitivity was subsequently enhanced through hydrogen plasma treatment. The SAW sensors were tested at H<sub>2</sub> and CH<sub>4</sub> at RT, and they exhibited a reversible response for both gases at concentrations between 0.02% and 0.1%, with a detection limit of a few ppm. The additional hydrogen plasma treatment preserved the lamellar structure, with slight modifications to the morphology of CNW edges, as observed by scanning electron microscopy (SEM). X-ray photoelectron spectroscopy (XPS) investigations revealed the presence of new functional groups, a significant number of defects and electron transitions after the treatment. Changes in the chemical state on the CNW surface are most probably responsible for the improved gas adsorption after plasma treatment. These results identify CNWs as a promising material for designing new SAW sensors, with the possibility of using plasma treatments to enhance the detection limit below the ppm level.

**Keywords:** carbon nanowalls; vertical graphene; surface acoustic waves; sensor; hydrogen; methane; plasma treatment



**Citation:** Vizireanu, S.; Constantinoiu, I.; Satulu, V.; Stoica, S.D.; Viespe, C. High-Sensitivity H<sub>2</sub> and CH<sub>4</sub> SAW Sensors with Carbon Nanowalls and Improvement in Their Performance after Plasma Treatment. *Chemosensors* **2023**, *11*, 566. <https://doi.org/10.3390/chemosensors11110566>

Academic Editor: Boris Lakard

Received: 26 October 2023

Revised: 14 November 2023

Accepted: 15 November 2023

Published: 16 November 2023



**Copyright:** © 2023 by the authors. Licensee MDPI, Basel, Switzerland. This article is an open access article distributed under the terms and conditions of the Creative Commons Attribution (CC BY) license (<https://creativecommons.org/licenses/by/4.0/>).

## 1. Introduction

The detection of dangerous substances is often necessary in many fields of activity, so the development of new sensors with good sensitivity and selectivity is an intensely debated topic. Both in research and in the industrial environment, there is a large category of sensors that are frequently used to detect dangerous gases: resistive sensors, metal-oxide semiconductor gas sensors, optical sensors, potentiometric sensors, capacitive sensors, etc. [1,2]. This category also includes surface acoustic wave (SAW) sensors [3,4]. SAW sensors respond to the physical characteristics of the gas species because they interact with the mechanical properties of the surface acoustic waves generated by the electric current applied to the piezoelectric substrate. Also, the characteristics of the surface acoustic waves are also influenced by the changes that take place on the sensitive layer of the SAW sensor. Thus, the electrical output signal is altered, identifying the presence of the analyte in the analyzed environment [5]. They stand out for their good sensitivity, reliability, short response and recovery times and the possibility of wireless operation and integration into a security system [6,7]. Also, considering that the sensitive element of this type of sensor can be realized from a wide range of materials (semiconductor metal oxides, metals, polymers,

composite materials, carbon nanotubes, carbon nanowalls, etc. [8]), it has the advantage of being adapted for a wide range of applications such as mechanical sensing, biological sensing, chemical sensing, gas sensing and microfluidics. Regarding gas detection, it can be used both for organic gases (methane (CH<sub>4</sub>), ethanol, dichloroethane) and for inorganic gases (nitrogen, ozone), including volatile organic compounds (toluene, ethanol, etc.), hydrogen (H<sub>2</sub>), nitrogen, hydrogen sulfide and chemical warfare agents [5,9,10].

The detection of H<sub>2</sub> at the lowest concentrations becomes more and more necessary due to the perspective of using it as a fuel, instead of fossil fuels [11]. H<sub>2</sub> has proven to be an environmentally friendly gas, but it comes with some challenges because it is a combustible gas at accumulations between 4% and 75%, with a diffusion coefficient in air of 0.60 cm<sup>2</sup>/s and an ignition energy of 0.002 mJ [12]. It is a colorless, odorless and tasteless gas, which implies the impossibility of being detected by human or animal sense organs. It is a gas with a very small molecule, which can very easily penetrate different materials, and therefore, it requires rigorous control of concentration in areas with a possible risk of accumulation. Thus, the need for artificial sensors to detect H<sub>2</sub> accumulation in air is increasing [12,13].

On the other hand, CH<sub>4</sub> is one of the most harmful gases, having a very high capacity to retain heat at the surface of the Earth [14]. The most dangerous areas for methane accumulation are coal mines. More recently, they have become a real danger to the environment as well due to the anaerobic processes in the landfill areas. An accumulation of 4–15% methane in air can cause explosions [15].

Consequently, these two gases require the safe and permanent control of their accumulation in different environments in society, through high-performance sensors. This requirement also comes with the need for detection at room temperature (RT) for safety because high temperatures contribute to accelerating the risk of explosion in a closed space with accumulations of the discussed gases.

The most important property of a sensitive material is to have the ability to suffer a measurable change following the interaction with the species to be detected. The most common interaction at the level of the sensitive layer is the adsorption of the analyte [5]. Carbon-based nanostructured materials represent one of the most studied categories of materials for sensor applications. Carbon nanotubes, carbon nanoparticles and graphene-based nanostructures are materials that have been used as a sensitive element for sensors for different types of gases [16,17]. However, in order to obtain the best possible detection limits, they were frequently used with other materials such as different polymers and different oxides, or they were used at a certain temperature to ensure sensitivity [18,19]. These things require a greater consumption of resources and energy.

It is known that both the morphology of the sensitive material and its structural characteristics influence the performance of a sensor [2,20]. Besides the use of single graphene in electronic devices, we can find many tests conducted on other multilayered graphene-based materials, especially vertically aligned ones [21,22].

We consider that vertically oriented graphene (VOG) layers [23] could achieve great performance in the field of SAW equipment. These nanomaterials (VOG) can be found in the literature under several names: carbon nanowalls (CNWs) [24], carbon nanoflakes [25], nanosheets [26], few layers of graphene, vertically aligned few-layer graphene [27], 2D nano-graphite sheets, nano-graphite crystallites [28], etc. These VOG or CNW-type nanostructures have numerous characteristics derived from their basic structure, multilayer graphene, as well as from their specific morphology, architecture and geometry (quasi-two-dimensional) with sharp edges and a large specific area, over 1000 m<sup>2</sup>/g [29]. These nanostructures generally show a semi-metallic behavior at RT, while they have a semiconductor character at low temperatures [30]. A large part of CNW characteristics (transport, morphology, structures, surface chemistry, etc.) can be controlled directly from the synthesis process, but they can also be modified later through post-synthesis treatments [31]. Plasma functionalization [31] and decoration [32,33] are the most effective post-synthesis methods in the control and modification of their characteristics.

In the case of detection applications, CNW-like materials can be considered among the most promising nano/micro-porous structures, especially due to the large specific surface area, their sharp edges and their electronic mobility. These layers present sensitivity like that of single graphene, especially in the area of sharp edges, where there are only a few graphene layers (2–5 graphene layers), compared to the base. According to the detection mechanism, we can list several types of sensors based on vertically oriented graphene: chemo-resistive sensors [34], electrochemical sensors [35,36], SERS sensors (based on Raman amplification by the surface plasmons on the CNW surface) [32], MR sensors (magneto-resistive-based on the magneto-transport phenomenon present in CNWs) [37] and SAW sensors (based on surface acoustic wave modulation), but for the latter there are no reports on CNW-type materials. In our previous reports [32,34], we presented the detection limits and analytes detectable using the SERS method and also the representative examples of gas/vapor detection ( $H_2$ ,  $NH_3$ ,  $NO_2$ , acetone vapors, methanol, diethyl ether, iso-pentanol) by CNWs and CNW hybrid chemo-resistive sensors and their performance.

In the present study, a SAW sensor with a CNW sensitive layer was fabricated via plasma-enhanced chemical vapor deposition (PECVD) by using a low-pressure RF plasma jet. Further, this sensor was treated in  $H_2$  plasma. The advantages of this method are the possibility of controlling the synthesis parameters, the use of a low growth temperature (because of the energy provided by plasma, the need for a high temperature is reduced), a fast reaction rate and high efficiency [38,39].

To the best of our knowledge, (from the literature dedicated to vertically oriented graphene), there has been no report/study about SAW sensors based on CNWs. On the other hand, the plasma treatment approach is another topic of interest and novelty in this paper. By using  $H_2$  plasma treatment, we managed to improve the sensitivity of the initial sensor. After the initial gas tests/measurements of the sensor based on CNW layers on SAW electrodes, the CNW layers were treated in  $H_2$  plasma, and we observed that the sensitivity was improved.

By using SAW sensors with CNWs as an active material, we can succeed in the detection of  $H_2$  and  $CH_4$  in the range of 4 ppm and 14 ppm, respectively. Compared to other results of SAW sensors obtained in our laboratory and tested in the detection of  $H_2$  at RT, these are tens of times better. The best LOD in [40] was 251 ppm, and in [2], the best LOD was 1210 ppm.

To highlight the importance of using vertical graphene in the fabrication of SAW-type sensors, we compare the present results with other  $H_2$  and  $CH_4$  sensors based on graphene from the literature. We identified some reviews that present the state of the art with a table and comparison of representative results for  $H_2$  [12] and  $CH_4$  [41] sensors based on graphene layers and many combinations between graphene and metallic nanoparticles or polymers. By adding nanoparticles (decoration) and mixing graphene with polymers, the detection limit can be enhanced. Some examples [12] of chemoreceptive  $H_2$  sensors show the possibility of detecting  $H_2$  in the small quantity of 100 ppm and concentrations as low as 0.025–1% in synthetic air at RT by using sensors based on graphene composites with polymers (PEDOT:PSS, PANI, PMMA) or detecting  $H_2$  at even lower concentrations by using sensors based on graphene composites with metals (20 ppm of  $H_2$  using Pd/graphene (RT), 1%  $H_2$  using Pt/graphene (RT) and 0.5%  $H_2$  using Pt/reduced graphene oxide (RGO) as sensitive materials working at 50 °C). Chemo-resistive  $H_2$  sensors based on modified graphene with metal (Pd/graphene composite) could have detection limits below 0.1 ppm [42]. When the same sensitive material, Pd/graphene, was used for the fabrication of resistive and SAW sensors, tests showed a better detection performance for the resistive sensor, which detected a minimum  $H_2$  concentration of 0.2 ppm; in contrast, the lowest concentration detected by the SAW sensor was 0.25% (2500 ppm) [42].

In addition, SAW sensors based on graphene and their composites are also sensitive to other species such as humidity [43,44], NO [45] and TNT [46].

As we described above, the use of graphene-based composites leads to an increase in the performance of SAW sensors. It is difficult to identify studies regarding the fabrication

of SAW sensors used in H<sub>2</sub> and CH<sub>4</sub> detection by using only simple, unmodified graphene multilayers (no metal or polymer composites) as sensitive materials. However, we can list a few reports on H<sub>2</sub> detection and one study on CH<sub>4</sub> detection (Table 1).

**Table 1.** Results of SAW sensors based on graphene layers.

Sensitive Layer	Analyte	Concentration	Working Temperature	Reference
Reduced graphene oxide	H <sub>2</sub> /Ar H <sub>2</sub> in synthetic air	100 ppm 1000 ppm	RT	[47]
Graphene oxide layers	H <sub>2</sub> in synthetic air NO <sub>2</sub> in synthetic air	4–75% 125 ppm	20–120 °C	[48]
Graphene-like nano-sheets	H <sub>2</sub> CO	1% 1000 ppm	25 °C	[9]
Graphene–nickel–cryptophane	CH <sub>4</sub>	1%	RT	[49]
CNW—vertical graphene	H <sub>2</sub> CH <sub>4</sub>	7.9 ppm 4.3 ppm	RT	Actual work

## 2. Materials and Methods

### 2.1. Synthesis of CNWs and Their Plasma Treatment

The vertically aligned graphene or CNW layer was synthesized using a low-pressure RF plasma jet in a mixture of gases of Ar/H<sub>2</sub>/C<sub>2</sub>H<sub>2</sub> at a ratio of 1000/25/2 SCCM (standard cubic centimeters per minute) in a working pressure of about 110 Pa [50]. The radio frequency power was set at 300 W for 30 min deposition time. The deposition was performed on SAW sensor quartz substrates (SAW@CNW), and the temperature was maintained at 600 °C during deposition. After the SAW@CNW sensor was tested (the description of the testing process is below), its sensitive CNW layer was subjected to H<sub>2</sub> plasma treatment in order to improve the performance of the sensor (SAW@CNW\_Treat). This treatment was performed in Ar/H<sub>2</sub> plasma at a gas ratio of 100/50 sccm, at a pressure of 5 Pa, at 100 W, for 600 °C for 30 min of treatment. The sensitive layer of the sensor was morphologically and compositionally characterized by SEM and XPS before and after H<sub>2</sub> plasma treatment. For SEM, we used an Apreo S Thermo Fisher Scanning Electron Microscope (Thermo Scientific, Waltham, MA, USA), with a maximum resolution of 0.7 nm. The SEM images were recorded at a working voltage of 15 kV. X-ray photoelectron spectroscopy (XPS) was performed using a K-Alpha Thermo Scientific (ESCALAB™ XI+, East Grinstead, UK) spectrometer equipped with a monochromatic Al K $\alpha$  X-ray source (1486.6 eV). The acquisition steps were 1 eV for the general spectra and 0.1 eV for high-resolution spectra.

### 2.2. Sensor Structure and Testing

The delay-line SAW sensor consisted of a quartz piezoelectric substrate, two pairs of gold interdigital transducers (IDTs) and a sensitive layer (Figure 1). The ST-X-cut quartz substrate had a parallelogram geometry, which contributed to the reduction in unwanted SAW reflections and a relatively low temperature coefficient [51]. The SAW sensor was 38 mm long, 10 mm wide and 0.5 mm thick. The IDTs were made of 50 electrode pairs, placed in a double-comb configuration with a periodicity of 11  $\mu$ m (Figure 1). They had a thickness of 150 nm, and they were deposited by photolithography, on a chrome layer that ensures the adhesion of the gold on the quartz substrate. The deposition of the sensitive layer was limited using a mask that protected the IDTs.

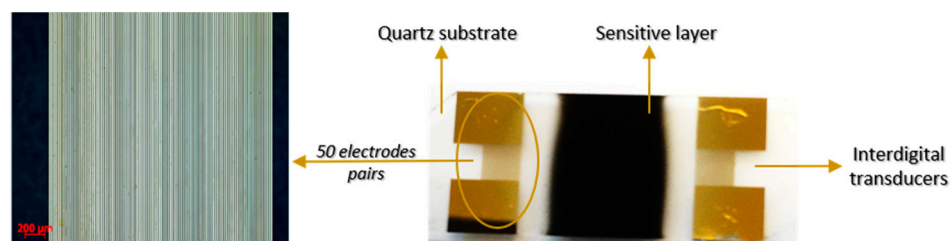


**Figure 1.** Scheme of the SAW sensor with CNW sensitive layer.

As the substrate is piezoelectric, when an incoming electrical radiofrequency signal is applied to the IDTs, it is converted into mechanical waves. They cross the surface of the SAW sensor to the other pair of IDTs, with a certain oscillation frequency. This oscillation frequency is perturbed when the properties of the sensitive layer are modified due to the presence of the gas molecules. These changes result from mass accumulation of gas molecules in the sensitive layer, or due to electrostatic interactions with the sensitive layer [5,51].

The sensors were tested at concentrations between 0.02% and 0.1%  $H_2$  and  $CH_4$ . These concentrations were obtained by homogenizing the target gas mixtures of  $H_2$  and  $CH_4$  with synthetic air, using three mass flow meters connected to a mass flow controller. The gas flow rate was maintained constant at 0.5 L/min. The temperature and the gas flow rate were maintained constant during all measurements, in order not to induce the cooling of the substrate, which would be a second factor for changing the frequency shift, apart from the ad/absorption of gas molecules in the sensitive layer.

The test results were processed using Times View 3 software, connected to a DHPVA-200 FEMTO amplifier (Messtechnik GmbH, Berlin, Germany) and a CNT-91 Pendulum Frequency Counter (Figure 2). More details about the sensor test system and experimental setup are presented in Figure 2 and in [40].

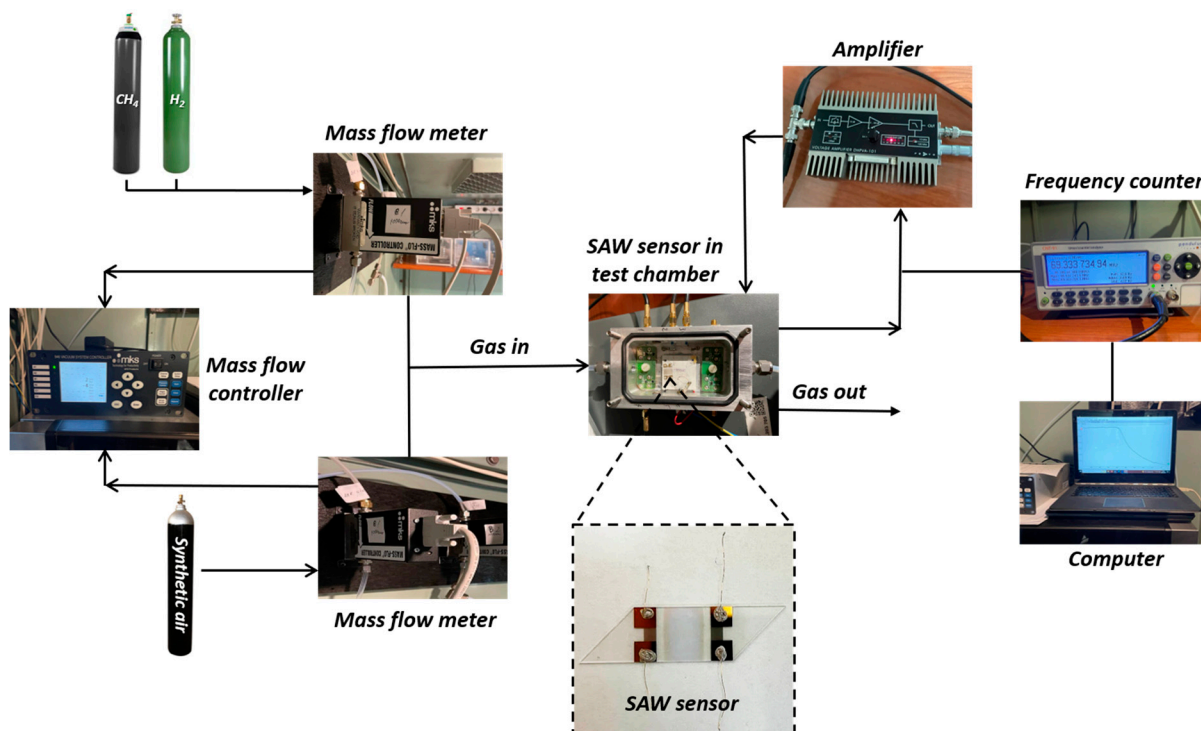


**Figure 2.** Experimental setup for SAW sensor measurements.

### 3. Results and Discussion

The morphology of the CNW film deposited on the SAW electrode is shown in Figure 3a. It is a typical top-view morphology of CNWs (lamellar network) and is similar to the morphology of CNWs usually obtained before for a temperature of 700 °C at the same Ar/H<sub>2</sub>/C<sub>2</sub>H<sub>2</sub> ratio [16]. The H<sub>2</sub> plasma treatment modifies the morphology, as we can see in Figure 3b, while surface chemistry is also changed, as we will see below. In Figure 3b, we can notice a thickening of the individual edges of the CNWs [52] and on the other hand, we can see that the inter-spaces between the walls seem to be emptier compared to those of the initial sample. We can say that the H<sub>2</sub> plasma treatment led to the etching of edge tips, but also to the corrosion of the carbonic materials between the walls of the CNW layers, as can be seen in Figure 3b. After the sensor tests, the device was fragmented for cross-section SEM investigation. From the cross-section image, the thickness of treated CNW layers was determined to be about 500 nm.

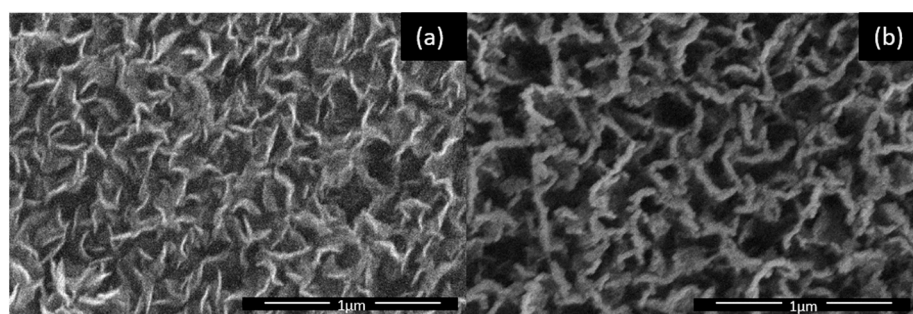


Figure 3. SEM images of (a) SAW@CNW sensor and (b) SAW@CNW\_Treat.

The XPS survey spectra provide valuable insights into SAW@CNW sample composition and plasma treatment effects on surface properties, which are necessary for advanced materials development. Figure 4 shows the XPS survey spectra of both samples—the as-deposited SAW@CNW and the SAW@CNW\_Treat samples. An analysis of the spectra reveals that both samples are mainly composed of carbon, oxygen, and nitrogen. The chemical composition of these samples is presented in Table 2, which provides detailed information on the peak positions of these elements and their relative atomic concentrations. Upon plasma treatment, we observed a noticeable increase in oxidation and the introduction of more oxygen- and nitrogen-containing chemical groups. This change in composition (introductions of more oxygen and nitrogen atoms) is most likely due to the low vacuum during treatment and subsequent exposure to the atmosphere.

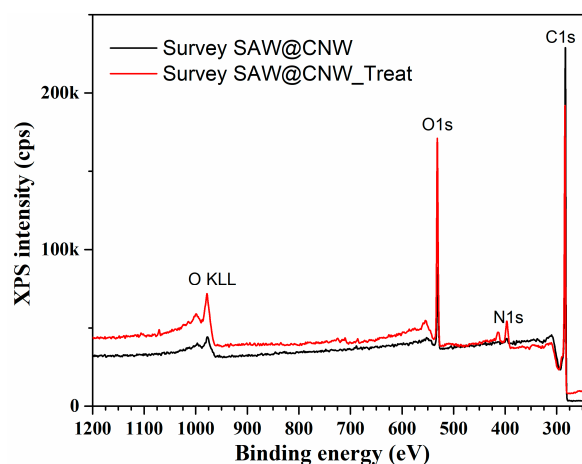
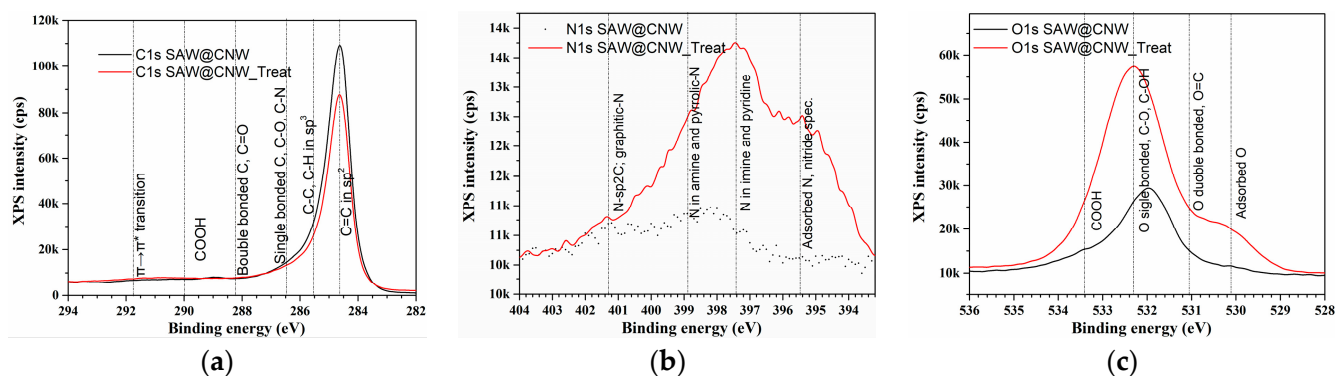


Figure 4. The XPS general spectra of SAW@CNW and SAW@CNW\_Treat.

**Table 2.** The relative atomic concentration and the peak position for CNWs and plasma-treated CNWs deposited onto SAW electrodes.

Sample	Name	Position	% Conc.
SAW@CNW	C 1s	284.6	89.6
	N 1s	398.6	1.3
	O 1s	532.6	9.1
SAW@CNW_Treat	C 1s	284.6	70.2
	N 1s	397.6	7.3
	O 1s	532.6	22.5

A detailed analysis was conducted using high-resolution XPS to investigate the connection of various elements to the material's surface. The study was focused on the carbon region C1s, but the N1s and O1s regions were also recorded. Figure 5 presents the high-resolution spectra in these regions and (with a dotted line) the positions (binding energy) of the most probable chemical bonds, as assigned previously [41] or identified by other authors for this type of nanomaterial [53]. The overlay of these spectra revealed significant modifications in chemical states after treatment. Although the difference may not be obvious in the overlap graphs of the C1s region of carbon in Figure 5a, the changes become more apparent after deconvolution of the graphs (Figure 6) and calculation of the relative percentages of each component. On the other hand, it is quite evident (Figure 5b,c) that in the N1 and O1s regions, an important contribution is found as adsorbed nitrogen (at about 395.6 eV) and oxygen (at 530.1 eV), possibly as molecules trapped between the walls after treatment. The other bonds made by nitrogen after the plasma treatment at 600 °C are of the N pyrrolic and pyridinic type (with binding energy at ~397.5 and 398.9 eV), with a small amount as graphitic N (~401.3 eV). Similarly, the rest of the oxygen bonds are of the O= double bond (as in O<sub>2</sub> and CO<sub>2</sub> at about 531.1 eV), O- single bond (532.3 eV) and COOH (at 533.4 eV) types.

**Figure 5.** High-resolution XPS spectra of CNWs and treated CNWs in the region of (a) C1s, (b) N1s and (c) O1s.

The C1s region is worth further discussion, as the other chemical groups are linked to the carbonic base structure. The C1s region of the sample was analyzed in detail, and it was found to contain six distinct sub-peaks, namely C1, C2, C3, C4, C5 and C6, with their respective energy levels centered at about 284.6 eV, 285.6 eV, 286.5 eV, 288.4 eV, 290.0 eV, and 291.8 eV, after calibration of the initial C1s peak at 284.6 eV. These sub-peaks were assigned to specific chemical components, with C1 representing the C=C in sp<sup>2</sup>; C2 assigned to single bonded C- as C-C in sp<sup>3</sup> or in defects and C-H; C3 representing C-OH, O-C-O and C-N; C4 attributed to double-bonded C= as C=O; C5 representing O=C-OH; and C6

assigned to delocalized orbitals also known as  $\pi$ - $\pi^*$  transitions. The relative concentration of each component in the C1s spectra was further analyzed, and the results are presented in Figure 6.

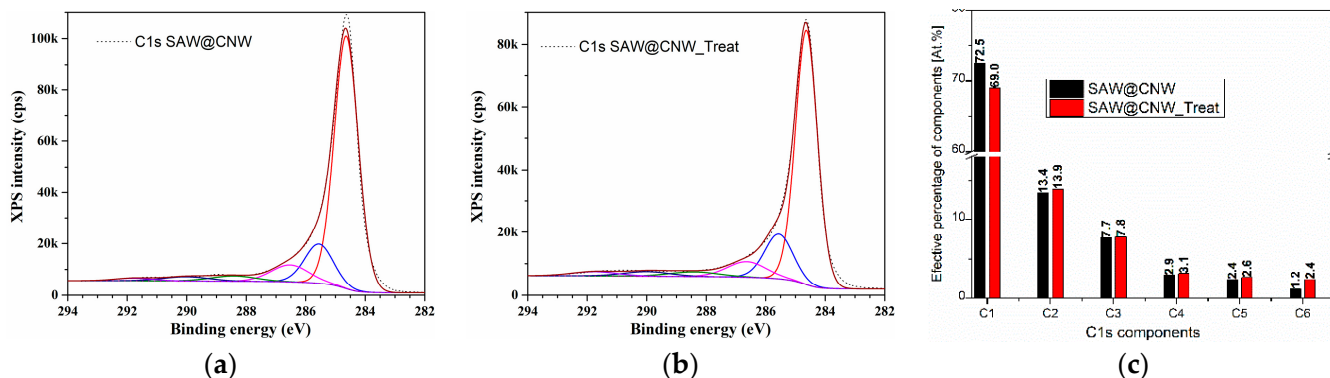


**Figure 6.** C1s high-resolution XPS spectra (dotted lines) and their deconvolution (subpeaks with color lines: C1-red line; C2-blue line, C3-magenta line, C4-olive line, C5-navy line, C6-purple line) for (a) SAW@CNW and (b) SAW@CNW\_Treat and (c) the relative percentages of C1–C6 components of these samples.

It was observed that there was a decrease in the relative concentration of C=C in  $sp^2$  groups and an increase in the relative concentration of C-C in  $sp^3$  and defects, as well as COOH groups and the  $\pi$  transition. The increase in the number of electrons in the  $\pi$  orbitals reflects some change in the conduction band of materials. Surface chemistry modifications have a pronounced effect on the absorption of diverse molecules that are detected by the materials. This was confirmed by sensor tests on two types of gases,  $H_2$  and  $CH_4$ , after plasma treatment.

The tests were carried out at concentrations of gases between 0.02% and 0.1% and at RT. The calculated relative error was less than 4% for more than 20 consecutive measurements for the same concentrations. The oscillation frequency of the sensors was about 62 MHz. The noise level of the SAW sensor (in both cases, untreated and treated CNWs) was 25 Hz.

The sensors tested in the detection of  $H_2$  had responses for each concentration tested, and the graph of frequency shifts (Figure 7) shows that there was an improvement in sensor response after the plasma treatment. The same trend was observed both for sensitivity and limit of detection (LOD). Sensitivity represents the frequency shift in Hz per unit analyte concentration in ppm [2,51]. LOD is defined as 3 times the noise level divided by the sensitivity [2,51]. Table 3 confirms this, showing an increase in the sensitivity and a decrease in the limit of detection (LOD) of the sensor after the plasma treatment, by approximately 68% and 41%, respectively, compared to the results before this treatment. The average sensitivity before the plasma treatment was 5.62 Hz/ppm, and the average sensitivity increased to 9.4 Hz/ppm after the plasma treatment. Regarding LOD, it decreased from 13.35 ppm before treatment to 7.79 ppm after plasma treatment. Also, the response time decreased after the plasma treatment, from 80 s to 75 s. We suppose that the improvement in SAW performance after plasma treatment is closely related first of all to the presence of more electrons in the  $\pi$  orbitals (1.2%) and to the increase in the percentage of defects and CH bonds (0.5%), C-O/C-N bonds (0.1%), C=O bonds (0.2%) and COOH bonds (0.2%), as shown in Figure 6c.

Results were also obtained for  $CH_4$ , for all concentrations tested at RT. Compared to the frequency shifts obtained for  $H_2$ , those for  $CH_4$  were doubled (Figure 8).

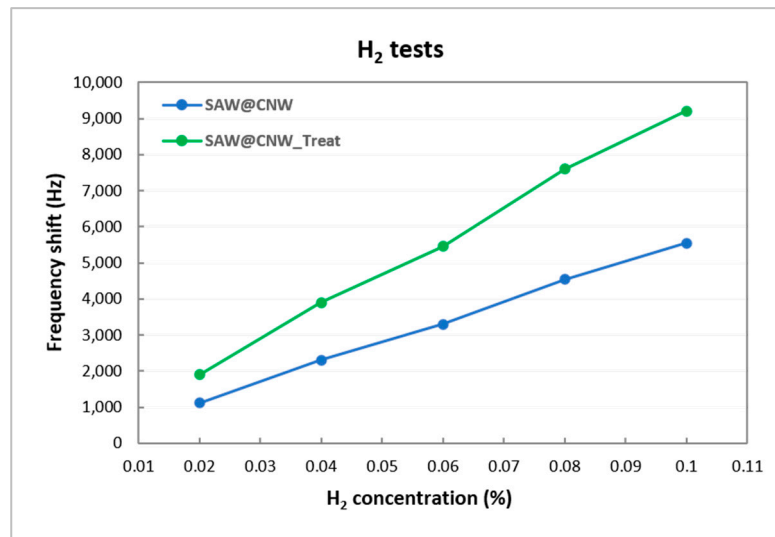


Figure 7. Frequency shift of the SAW sensor at different H<sub>2</sub> concentrations.

Table 3. Sensitivity and limit of detection (LOD) of the sensor in H<sub>2</sub> tests. Legend:  $\Delta f$ —frequency change;  $c$ —H<sub>2</sub> concentration;  $n$ —noise level.

H <sub>2</sub> (%)	Sensitivity ( $\Delta f/c$ ) (Hz/ppm)		LOD ( $3\sigma_n/(\Delta f/c)$ ) (ppm)	
	Before Plasma Treatment	After Plasma Treatment	Before Plasma Treatment	After Plasma Treatment
0.02	5.6	9.5	13.39	7.89
0.04	5.78	9.75	12.99	7.69
0.06	5.5	9.08	13.64	8.26
0.08	5.68	9.5	13.22	7.89
0.1	5.55	9.2	13.51	8.15

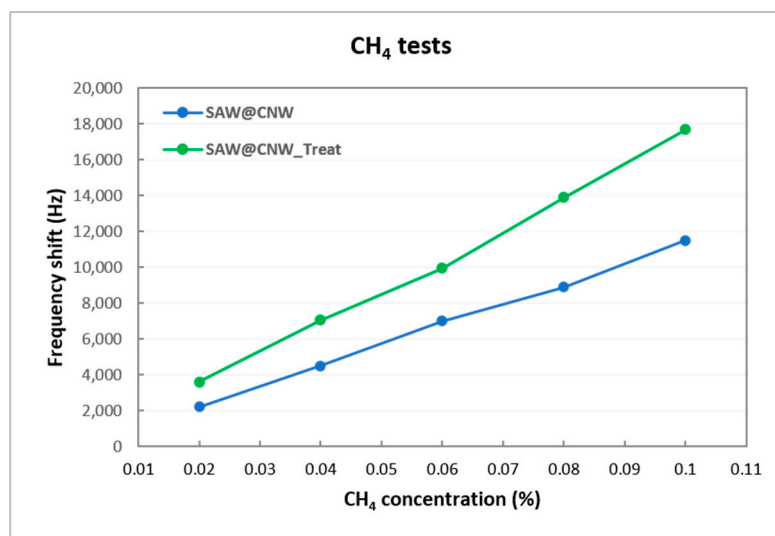


Figure 8. Frequency shift of the SAW sensor at different CH<sub>4</sub> concentrations.

Also, the results for sensitivity and LOD were twice better for CH<sub>4</sub> than for H<sub>2</sub>.

The average sensitivity to CH<sub>4</sub> obtained before the plasma treatment was 11.31 Hz/ppm; after the treatment, there was an increase of 54%, with the average sensitivity obtained being 17.46 Hz/ppm (Table 4). Regarding the LOD, the average obtained was 6.64 ppm before the plasma treatment, decreasing to 4.3 after it.

**Table 4.** Sensitivity and limit of detection (LOD) of the sensor in CH<sub>4</sub> tests. Legend:  $\Delta f$ —frequency change; c—H<sub>2</sub> concentration; n—noise level.

CH <sub>4</sub> (%)	Sensitivity ( $\Delta f/c$ ) (Hz/ppm)		LOD ( $3xn)/(\Delta f/c)$ (ppm)	
	Before Plasma Treatment	After Plasma Treatment	Before Plasma Treatment	After Plasma Treatment
0.02	11.00	18.00	6.82	4.17
0.04	11.25	17.63	6.67	4.26
0.06	11.67	16.58	6.43	4.52
0.08	11.13	17.38	6.74	4.32
0.1	11.50	17.70	6.52	4.24

The better response of the sensor for CH<sub>4</sub> than for H<sub>2</sub> (in both cases, untreated and treated CNWs) is explained by the good adsorption and CH<sub>4</sub> molecules possibly trapped between the layers of CNW.

The CH<sub>4</sub> adsorption is improved on the CNW surface due to the “Effects of Graphene Stacking” [54] that appear in the multilayer graphene structure of CNW layers due to  $\pi$  electrons, but also due to the presence of defects, activation [55] and dopants [56]. On the other hand, Van der Waals forces must be considered in CH<sub>4</sub> molecule adsorption, as they are considered in the calculation of adsorption energies of methane molecules on graphene with defects and dopants [56]. On the other hand, another explanation could be that under the same conditions of temperature and pressure (RT and atmospheric pressure), but also on the same sensitive element, CNWs, CH<sub>4</sub> has a higher molecular mass (larger and heavier molecule) than H<sub>2</sub> and “sits” with a larger mass on the sensitive element, and also the direct interaction with the surface acoustic waves is more pronounced in its case.

From the dynamic response of SAW@CNW\_Treat in the H<sub>2</sub> test (Figure 9), it can be seen that the sensor is a reversible one, which returns to the initial oscillation frequency after the release of the gas of interest. This is another important feature for sensor performance and most of the time is an advantage of SAW sensors. Due to the fact that there is no irreversible chemical reaction with the gas molecules on the sensitive layer, desorption occurs after the release of the gas, which allows the sensor to be used for other determinations.

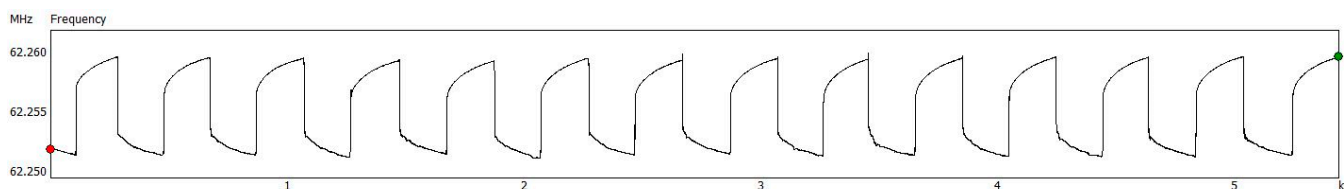


**Figure 9.** Dynamic response of SAW@CNW\_Treat at 800 ppm H<sub>2</sub> gas concentration.

The results show a significant improvement in the absorption of these gases by the plasma-treated CNWs, highlighting the potential of surface chemistry modifications in enhancing the performance of SAW sensors.

#### 4. Conclusions

We successfully grew a sensitive layer based on vertically aligned graphene on a SAW substrate using a low-pressure RF plasma jet at 600 °C. Later, the sensitive layer was subjected to H<sub>2</sub> plasma treatment to observe its influence on the SAW sensor response. Both the SAW@CNW and SAW@CNW\_Treat sensors responded to H<sub>2</sub> and CH<sub>4</sub> at concentrations between 0.02% and 0.1%. It was observed that there was an improvement in detection after plasma treatment for both gases, the best sensitivity being obtained by the SAW@CNW\_Treat sensor tested for CH<sub>4</sub>, with an average of 17.45 Hz/ppm and an LOD of 4.3 ppm, at RT.

Hydrogen plasma treatment led to the etching of CNW edges and cleaned the space between the walls, but the lamellar structure was preserved, as we saw in the SEM investigation. Instead, we highlight the changes in the chemistry of the CNW surfaces. The appearance of new chemical groups and the increase in defects and electron transitions contribute to the large absorption of gases on treated CNWs, which enhances the sensitivity.

These results are promising for the development of new SAW sensors based on vertically aligned graphene layers that work at RT, with performances below the ppm level. On the other hand, the testing of new plasma treatments should be considered for improving the performance of other SAW sensors.

**Author Contributions:** Conceptualization, C.V. and S.V.; methodology, C.V., S.V. and I.C.; formal analysis, V.S., S.D.S. and I.C.; investigation, S.V., V.S., S.D.S., I.C. and C.V.; writing—original draft preparation, S.V., I.C. and C.V.; writing—review and editing, S.V., I.C. and C.V. All authors have read and agreed to the published version of the manuscript.

**Funding:** This work was supported by Romanian Ministry of Research, Innovation and Digitization through the project PN-III-P2-2.1-PED-2021-2559, contract No. 632 PED/2022 BIOPLASM, and the project CNCS—UEFISCDI, PCE 93/2021 PN-III-P4-ID-PCE-2020-1822 within PNCDI III and Romanian National Core Program LAPLAS VII contract No. 30N/2023 of National Institute for Lasers, Plasma and Radiation Physics.

**Institutional Review Board Statement:** Not applicable.

**Informed Consent Statement:** Not applicable.

**Data Availability Statement:** Data are contained within the article.

**Conflicts of Interest:** The authors declare no conflict of interest.

#### References

1. Constantinoiu, I.; Viespe, C. Detection of Volatile Organic Compounds Using Surface Acoustic Wave Sensor Based on Nanoparticles Incorporated in Polymer. *Coatings* **2019**, *9*, 373. [[CrossRef](#)]
2. Constantinoiu, I.; Viespe, C. Development of Pd/TiO<sub>2</sub> Porous Layers by Pulsed Laser Deposition for Surface Acoustic Wave H<sub>2</sub> Gas Sensor. *Nanomaterials* **2020**, *10*, 760. [[CrossRef](#)] [[PubMed](#)]
3. Pan, Y.; Wang, P.; Zhang, G.; Yan, C.; Zhang, L.; Guo, T.; Wang, W.; Zhai, S. Development of a SAW poly(epichlorohydrin) gas sensor for detection of harmful chemicals. *Anal. Methods* **2022**, *14*, 1611. [[PubMed](#)]
4. Li, Y.; Xiao, A.S.; Zou, B.; Zhang, H.X.; Yan, K.L.; Lin, Y. Advances of metal–organic frameworks for gas sensing. *Polyhedron* **2018**, *154*, 83–97.
5. Mandal, D.; Banerjee, S. Surface Acoustic Wave (SAW) Sensors: Physics, Materials and Applications. *Sensors* **2022**, *22*, 820.
6. Zhao, L.; Che, J.; Cao, Q.; Shen, S.; Tang, Y. Highly Sensitive Surface Acoustic Wave H<sub>2</sub>S Gas Sensor Using Electron-beam-evaporated CuO as Sensitive Layer. *Sens. Mater.* **2023**, *35*, 2293–2304.
7. Longa, G.; Guoa, Y.; Lib, W.; Tanga, Q.; Zua, X.; Mac, J.; Duc, B.; Fud, Y. Surface acoustic wave ammonia sensor based on ZnS mucosal-like nanostructures. *Microelectron. Eng.* **2020**, *222*, 111201.
8. Li, H.; Li, M.; Kan, H.; Lia, C.; Quan, A.; Fu, C.; Luo, J.; Liu, X.; Wang, W.; Yang, Z.; et al. Surface acoustic wave NO<sub>2</sub> sensors utilizing colloidal SnS quantum dot thin films. *Surf. Coat. Technol.* **2019**, *362*, 78–83.
9. Arsat, R.; Breedon, M.; Shafiei, M.; Spizziri, P.G.; Gilje, S.; Kaner, R.B.; Kalantar-Zadeh, K.; Wlodarski, W. Graphene-like nano-sheets for surface acoustic wave gas sensor applications. *Chem. Phys. Lett.* **2009**, *467*, 344–347.
10. Constantinoiu, I.; Viespe, C. ZnO Metal Oxide Semiconductor in Surface Acoustic Wave Sensors: A review. *Sensors* **2020**, *20*, 5118.
11. Kim, S.; Singh, G.; Lee, K. Development of Highly Sensitive and Stable Surface Acoustic Wave-Based Hydrogen Sensor and Its Interface Electronics. *Adv. Mater. Technol.* **2022**, *7*, 2200180. [[CrossRef](#)]

12. Ilnicka, A.; Lukaszewicz, J.P. Graphene-Based Hydrogen Gas Sensors: A Review. *Processes* **2020**, *8*, 633. [[CrossRef](#)]
13. Wang, X.; Du, L.; Cheng, L.; Zhai, S.; Zhang, C.; Wang, W.; Liang, Y.; Yang, D.; Chen, Q.; Lei, G. Pd/Ni nanowire film coated SAW hydrogen sensor with fast response. *Sens. Actuators B Chem.* **2022**, *351*, 130952. [[CrossRef](#)]
14. Zhuang, J.; Tian, Y. Dynamics of methane and other greenhouse gases flux in forest ecosystems in China. *J. Environ. Sci. Health Part A* **2021**, *56*, 241–247. [[CrossRef](#)]
15. Kwasny, M.; Bombalska, A. Optical Methods of Methane Detection. *Sensors* **2023**, *23*, 2834. [[CrossRef](#)]
16. Ge, W.; Pei, L.; Liu, Y.; Baktur, R. Carbon-nanotube-loaded planar gas and humidity sensor. *Microw. Opt. Technol. Lett.* **2020**, *62*, 3857–3863. [[CrossRef](#)]
17. Guo, S.Y.; Hou, P.X.; Zhang, F.; Liu, C.; Cheng, H.M. Gas Sensors Based on Single-Wall Carbon Nanotubes. *Molecules* **2022**, *27*, 5381. [[CrossRef](#)]
18. Wang, B.; Zhou, L.; Wang, X. Surface acoustic wave sensor for formaldehyde gas detection using the multi-source spray-deposited graphene/PMMA composite film. *Front. Mater.* **2023**, *9*, 1025903.
19. Xu, S.; Zhang, R.; Cui, J.; Liu, T.; Sui, X.; Han, M.; Zheng, F.; Hu, X. Surface Acoustic Wave DMMP Gas Sensor with a Porous Graphene/PVDF Molecularly Imprinted Sensing Membrane. *Micromachines* **2021**, *12*, 552. [[CrossRef](#)]
20. Miu, D.; Constantinoiu, I.; Enache, C.; Viespe, C. Effect of Pd/ZnO Morphology on Surface Acoustic Wave Sensor Response. *Nanomaterials* **2021**, *11*, 2598. [[CrossRef](#)]
21. Ahmada, R.; Majhi, S.M.; Zhang, X.; Swager, T.M.; Salama, K.N. Recent progress and perspectives of gas sensors based on vertically oriented ZnO nanomaterials. *Adv. Colloid Interface Sci.* **2019**, *270*, 1–27.
22. Roy, P.K.; Haider, G.; Chou, T.C.; Chen, K.H.; Chen, L.C.; Chen, Y.F.; Liang, C.T. Ultrasensitive Gas Sensors Based on Vertical Graphene Nanowalls/ SiC/Si Heterostructure. *ACS Sens.* **2019**, *4*, 406–412. [[CrossRef](#)] [[PubMed](#)]
23. Bo, Z.; Zhu, W.; Ma, W.; Wen, Z.; Shuai, X.; Chen, J.; Yan, J.; Wang, Z.; Cen, K.; Feng, X. Vertically oriented graphene bridging active-layer/current-collector interface for ultrahigh rate supercapacitors. *Adv. Mater.* **2013**, *25*, 5799–5806. [[CrossRef](#)]
24. Wu, Y.; Yang, B.; Zong, B.; Sun, H.; Shen, Z.; Feng, Y. Carbon nanowalls and related materials. *J. Mater. Chem.* **2004**, *14*, 469–477. [[CrossRef](#)]
25. Yao, Y.; Zhang, Y.; Li, L.; Wang, S.; Dou, S.; Liu, X. Fabrication of Hierarchical Porous Carbon Nanoflakes for High-Performance Supercapacitors. *ACS Appl. Mater. Interfaces* **2017**, *9*, 34944–34953. [[CrossRef](#)]
26. Zhao, X.; Tian, H.; Zhu, M.; Tian, K.; Wang, J.J.; Kang, F.; Outlaw, R.A. Carbon nanosheets as the electrode material in supercapacitors. *J. Power Sources* **2009**, *194*, 1208–1212. [[CrossRef](#)]
27. Malesevic, A.; Vitchev, R.; Schouteden, K.; Volodin, A.; Zhang, L.; Tendeloo, G.V.; Vanhulsel, A.; Haesendonck, C.V. Synthesis of few-layer graphene via microwave plasma-enhanced chemical vapour deposition. *Nanotechnology* **2008**, *19*, 305604. [[CrossRef](#)]
28. Kobayashi, K.; Tanimura, M.; Nakai, H.; Yoshimura, A.; Yoshimura, H.; Kojima, K.; Tachibana, M. Nanographite domains in carbon nanowalls. *J. Appl. Phys.* **2007**, *101*, 094306. [[CrossRef](#)]
29. Krivchenko, V.A.; Itkis, D.M.; Evlashin, S.A.; Semenenko, D.A.; Goodilin, E.A.; Rakhimov, A.T.; Stepanov, A.S.; Suetin, N.V.; Pilevsky, A.A.; Voronin, P.V. Carbon nanowalls decorated with silicon for lithium-ion batteries. *Carbon* **2012**, *50*, 1438–1442. [[CrossRef](#)]
30. Wu, Y.; Wang, H.; Choong, C. Growth of two-dimensional carbon nanostructures and their electrical transport properties at low temperature. *Jpn. J. Appl. Phys.* **2011**, *50*, 01AF02. [[CrossRef](#)]
31. Santhosh, M.N.; Filipič, G.; Kovacevic, E.; Jagodar, A.; Berndt, J.; Strunskus, T.; Kondo, H.; Hori, M.; Tatarova, E.; Cvelbar, U. N-Graphene Nanowalls via Plasma Nitrogen Incorporation and Substitution: The Experimental Evidence. *Nano-Micro Lett.* **2020**, *12*, 53. [[CrossRef](#)] [[PubMed](#)]
32. Mihai, S.; Cursaru, D.L.; Matei, D.; Dinescu, A.; Stoica, S.D.; Vizireanu, S.; Dinescu, G. Carbon nanowalls decorated with gold nanoparticles for surface-enhanced raman spectroscopy. *Dig. J. Nanomater. Biostruct.* **2018**, *13*, 743–749.
33. Kwon, S.; Kim, C.; Kim, K.; Jung, H.; Kang, H. Effect of Ag NPs-decorated carbon nanowalls with integrated Ni-Cr alloy microheater for sensing ammonia and nitrogen dioxide gas. *J. Alloy. Compd.* **2023**, *932*, 167551. [[CrossRef](#)]
34. Palla-Papavlu, A.; Vizireanu, S.; Filipescu, M.; Lippert, T. High-Sensitivity Ammonia Sensors with Carbon Nanowall Active Material via Laser-Induced Transfer. *Nanomaterials* **2022**, *12*, 2830. [[CrossRef](#)]
35. Wang, D.W.; Li, F.; Liu, M.; Lu, G.Q.; Cheng, H.M. 3D Aperiodic Hierarchical Porous Graphitic Carbon Material for High-Rate Electrochemical Capacitive Energy Storage. *Angew. Chem.* **2008**, *120*, 379–382. [[CrossRef](#)]
36. Shang, N.G.; Papakonstantinou, P.; McMullan, M.; Chu, M.; Stamboulis, A.; Potenza, A.; Dhessi, S.S.; Marchetto, H. Catalyst-free efficient growth, orientation and biosensing properties of multilayer graphene nanoflake films with sharp edge planes. *Adv. Funct. Mater.* **2008**, *18*, 3506–3514. [[CrossRef](#)]
37. Acosta Gentoii, M.; García Gutiérrez, R.; Alvarado Pulido, J.J.; Montaña Peraza, J.; Volmer, M.; Vizireanu, S.; Antohe, S.; Dinescu, G.; Rodriguez-Carvajal, R.A. Correlating Disorder Microstructure and Magnetotransport of Carbon Nanowalls. *Appl. Sci.* **2023**, *13*, 2476. [[CrossRef](#)]
38. Li, N.; Li, D.; Zhen, Z.; Zhang, R.; Mu, R.; Xu, Z.; He, L. Nucleation and growth of graphene at different temperatures by plasma enhanced chemical vapor deposition. *Mater. Today Commun.* **2023**, *36*, 106568. [[CrossRef](#)]
39. Li, N.; Zhen, Z.; Zhang, R.; Mu, R.; Xu, Z.; He, L. The nucleation and growth of graphene under a controlled atmosphere during radio frequency-plasma-enhanced chemical vapor deposition. *Vacuum* **2022**, *196*, 110750. [[CrossRef](#)]
40. Constantinoiu, I.; Miu, D.; Viespe, C. SAW Hydrogen Sensors with Pd/SnO<sub>2</sub> Layers. *Materials* **2022**, *15*, 8012. [[CrossRef](#)]

41. Hong, T.; Culp, J.T.; Kim, K.-J.; Devkota, J.; Sun, C.; Ohodnicki, P.R. State-of-the-art of methane sensing materials: A review and perspectives. *TrAC-Trends Anal. Chem.* **2020**, *125*, 115820. [[CrossRef](#)]
42. Ha, N.H.; Nam, N.H.; Dung, D.D.; Phuong, N.H.; Thach, P.D.; Hong, H.S. Hydrogen Gas Sensing Using Palladium-Graphene Nanocomposite Material Based on Surface Acoustic Wave. *J. Nanomater.* **2017**, *2017*, 905725. [[CrossRef](#)]
43. Balashov, S.M.; Balachova, O.V.; Braga, A.V.U.; Pavani Filho, A.; Moshkalev, S. Influence of the deposition parameters of graphene oxide nanofilms on the kinetic characteristics of the SAW humidity sensor. *Sens. Actuators B Chem.* **2015**, *217*, 88–91. [[CrossRef](#)]
44. Nikolaou, I.; Hallil, H.; Conedera, V.; Deligeorgis, G.; Dejous, C.; Rebiere, D. Inkjet-printed graphene oxide thin layers on love wave devices for humidity and vapor detection. *IEEE Sens. J.* **2016**, *16*, 7620–7627. [[CrossRef](#)]
45. Hung, T.-T.; Chung, M.-H.; Chiu, J.-J.; Yang, M.-W.; Tien, T.-N.; Shen, C.-Y. Poly(4-styrenesulfonic acid) doped polypyrrole/tungsten oxide/reduced graphene oxide nanocomposite films-based surface acoustic wave sensors for NO sensing behavior. *Org. Electron.* **2021**, *88*, 106006. [[CrossRef](#)]
46. Yang, J.; Wang, T.; Gao, W.; Zhu, C.; Yin, X.; Dong, P.; Wu, X. Surface Acoustic Wave Devices Based on Graphene Oxide/Au Nanorod Composites for Gas-Phase Detection of 2,4,6-Trinitrotoluene. *ACS Appl. Nano Mater.* **2022**, *5*, 12540–12551. [[CrossRef](#)]
47. Zhang, X.-Y.; Ma, R.-H.; Li, L.-S.; Fan, L.; Yang, Y.-T.; Zhang, S.-Y. A room-temperature ultrasonic hydrogen sensor based on a sensitive layer of reduced graphene oxide. *Sci. Rep.* **2021**, *11*, 2404. [[CrossRef](#)]
48. Drewniak, S.; Pustelny, T.; Setkiewicz, M.; Maciak, E.; Urbańczyk, M.; Procek, M.; Opilski, Z.; Jagiello, J.; Lipinska, L. Investigations of SAW structures with oxide graphene layer to detection of selected gases. *Acta Phys. Pol. A* **2013**, *124*, 402–405. [[CrossRef](#)]
49. Liu, X.; Shen, B.; Jiang, L.; Yang, H.; Jin, C.; Zhou, T. Study on SAW Methane Sensor Based on Cryptophane-A Composite Film. *Micromachines* **2023**, *14*, 266. [[CrossRef](#)]
50. Vizireanu, S.; Ionita, M.D.; Ionita, R.E.; Stoica, S.D.; Teodorescu, C.M.; Husanu, M.A.; Apostol, N.G.; Baibarac, M.; Panaitescu, D.; Dinescu, G. Aging phenomena and wettability control of plasma deposited carbon nanowall layers. *Plasma Process. Polym.* **2017**, *14*, 1700023. [[CrossRef](#)]
51. Ballantine, D.S.; White, R.M.; Martin, S.J.; Ricco, A.J.; Zellers, E.T.; Frye, G.C.; Wohtjen, H. *Acoustic Wave Sensors, Theory, Design, and Physico-Chemical Applications*; Academic Press: San Diego, CA, USA, 1997.
52. Kurita, S.; Yoshimura, A.; Kawamoto, H.; Uchida, T.; Kojima, K.; Tachibana, M.; Molina-Morales, P.; Nakai, H. Raman spectra of carbon nanowalls grown by plasma-enhanced chemical vapor deposition. *J. Appl. Phys.* **2005**, *97*, 104320. [[CrossRef](#)]
53. Bertóti, I.; Mohai, M.; László, K. Surface modification of graphene and graphite by nitrogen plasma: Determination of chemical state alterations and assignments by quantitative X-ray photoelectron spectroscopy. *Carbon* **2015**, *84*, 185–196. [[CrossRef](#)]
54. Yang, N.; Yang, D.; Zhang, G.; Chen, L.; Liu, D.; Cai, M.; Fan, X. The effects of graphene stacking on the performance of methane sensor: A first-principles study on the adsorption, band gap and doping of graphene. *Sensors* **2018**, *18*, 422. [[CrossRef](#)] [[PubMed](#)]
55. Zhu, Z.W.; Zheng, Q.R. Methane adsorption on the graphene sheets, activated carbon and carbon black. *Appl. Therm. Eng.* **2016**, *108*, 605–613. [[CrossRef](#)]
56. Islam, M.S.; Hussain, T.; Rao, G.S.; Panigrahi, P.; Ahuja, R. Augmenting the sensing aptitude of hydrogenated graphene by crafting with defects and dopants. *Sens. Actuators B Chem.* **2016**, *228*, 317–321. [[CrossRef](#)]

**Disclaimer/Publisher's Note:** The statements, opinions and data contained in all publications are solely those of the individual author(s) and contributor(s) and not of MDPI and/or the editor(s). MDPI and/or the editor(s) disclaim responsibility for any injury to people or property resulting from any ideas, methods, instructions or products referred to in the content.